Chapter 3

Low frequency dielectric measurements

3.1 Introduction

After about sixty years of lingering development [3, 211], low-frequency (LF) dielectric measurements are finally emerging as an important materials characterization tool. In the last few years, they have become indispensable in such diverse fields as:

- mining industry — for monitoring the quality of coal [212];
- pharmacological industry — for estimating adsorption of drugs onto nanoparticles for novel drug delivery systems [213];
- polymer industry — for monitoring the kinetics of polymerization in polymerizing systems [214, 215];
- oil industry — for estimating the water content in crude oil [216];
- biology — for online monitoring of cell concentrations during yeast cultivation and other fermentation processes [217, 218];

- medicine — for non-invasive measurements of tissues and bones, possibly leading to the development of diagnostic techniques for early detection of such maladies as cancer and osteoporosis [219, 220];
- material science — for optimization of the cure cycle of composites [3, 221]; and
- food science — for prediction of the level of cholesterol in certain food ingredients [222].

The LF dielectric measurements are unequaled in their ability to *dynamically* monitor the many chemical and physical processes important in investigations of new materials — such as cure, polymerization, phase transitions, and diffusion.

In this Chapter, we shall review the LF dielectric measurement techniques that we used to investigate the dielectric properties of fullerenes. Section 3.2 describes the conventional parallel-plate technique for measuring the dielectric function $\varepsilon(\omega)$. Sec. 3.3 deals with theoretical and practical considerations of *microdielectrometry*. Finally, Sec.3.4 discusses special techniques for high-impedance transport measurements. In addition, Appendix A contains the LabView code for the software written to control the measurement systems and instruments described in this section.

3.2 Parallel-plate measurements

3.2.1 Overview

The conventional way for making low frequency (below ~1 MHz) measurements of the dielectric properties of solids is to place a sample between closely spaced parallel conducting plates (Fig. 3-1), and to monitor the AC equivalent capacitance $C_m(\omega)$ and dissipation factor (also known as *loss tangent*) $D(\omega)$ of the resulting capacitor. Normally, one designs the plate spacing to be much less than the plate size, as this serves to minimize the effects of fringing field.

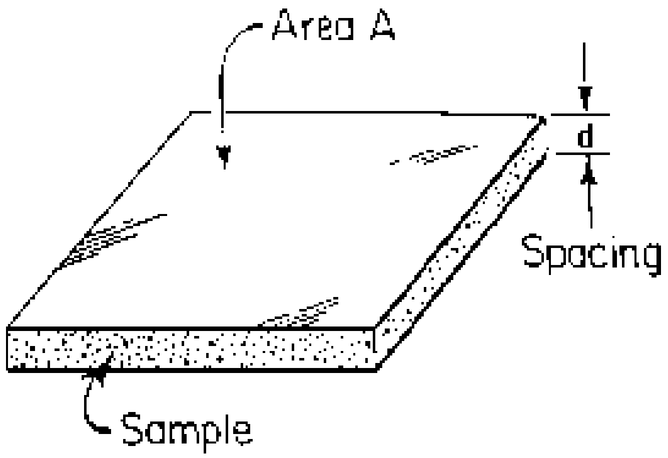

Figure 3-1: Parallel plate electrodes.

The material under test in the parallel-plate configuration (Fig. 3-1) can be modeled as a frequency-dependent capacitance $\mathbf{C}(\omega)$ in parallel with a frequency-independent resistor R_0 [Fig. 3-2(a)]. The DC resistance R_0 takes into account processes such as tunneling, thermally activated hopping, and ionic conduction. The capacitance $\mathbf{C}(\omega)$ is proportional to the complex dielectric function $\varepsilon(\omega) = \varepsilon'(\omega) - j\varepsilon''(\omega)$ of the sample material under test:

$$\mathbf{C}(\omega) = \varepsilon(\omega)\varepsilon_0 A/d, \tag{3.1}$$

where A is the cross sectional area of the capacitor, d is the separation between the plates, and $\varepsilon_0 = 8.85 \times 10^{-12}\,\mathrm{F/m}$ is the absolute permittivity of free space. The capacitance $C_m(\omega)$ measured by a typical capacitance bridge (such as an HP 4274A by Hewlett Packard, Inc. that was used in this study) is equal to the real part of $\mathbf{C}(\omega)$:

$$C_m(\omega) = \varepsilon'(\omega)\varepsilon_0 A/d, \tag{3.2}$$

and so it can be used to extract the frequency-dependent real part of the dielectric function $\varepsilon'(\omega)$. The other measured quantity, the dissipation factor (the *loss tangent*) given by

$$D(\omega) = \varepsilon''(\omega)/\varepsilon'(\omega) + \frac{d}{\omega\varepsilon_0\varepsilon'(\omega)AR_0}, \tag{3.3}$$

can then be used to extract the imaginary part of the dielectric function $\varepsilon''(\omega)$.

3.2.2 Special considerations

While the theory underlying the parallel-plate technique described above is quite simple, an actual measurement is complicated by a variety of additional constraints arising from the properties of the material being investigated, the nature of the interface, and the limitations of the measurement system. These three classes of constraints, as applied to the measurement of C_{60} solid films, are briefly discussed below.

Interfacial effects

In most actual measurements, the effect of *interfacial polarization* giving rise to the interfacial capacitance C_i needs to be taken into account. For a typical solid, the physics behind C_i includes:

1. The purely interfacial electronic effects influenced by the presence of electrons trapped with a finite lifetime in localized states near the interface [223], and

2. The "blocking layer" space-charge polarization effects due, *e.g.*, to the presence of mobile ions in the material [3, 193, 224] (see Fig. 3-3).

The measured capacitance C_m is then equal to the series combination of the interface capacitance C_i and the sample (bulk) capacitance C [225], as shown in Fig. 3-2(b). One thus expects the total reciprocal areal capacitance to have a linear dependence on thickness d of the sample with a *nonzero intercept* at $d = 0$, *i.e.*,

$$\frac{A}{C_m} = \frac{A}{C_i} + \frac{d}{\varepsilon_0\varepsilon'}. \tag{3.4}$$

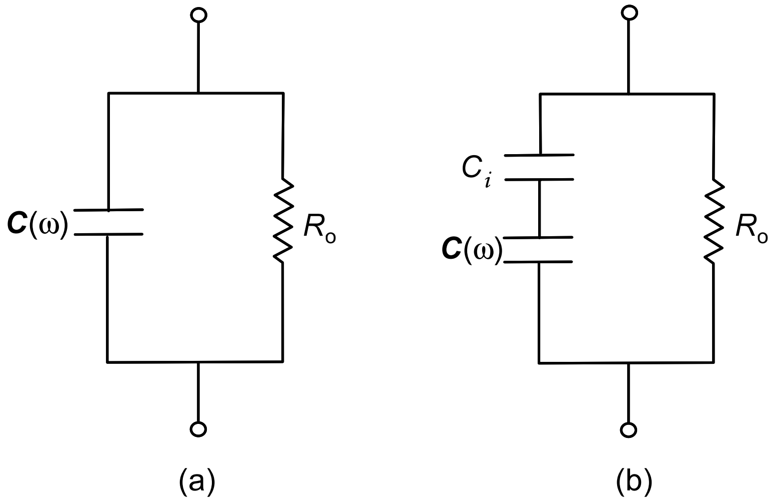

Figure 3-2: Equivalent circuits for the material under test in Fig. 3-1 with (b) and without (a) taking the interfacial capacitance into account.

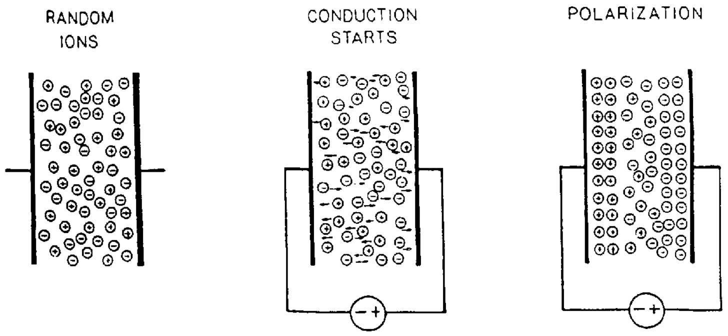

Figure 3-3: Idealized view of the polarization due to ions. Ion conduction in the presence of an applied electric field leads to electrode (interfacial) polarization and formation of a "blocking layer" (after Day *et al.* [193]).

Note that as the thickness d of the film gets smaller, the interfacial capacitance C_i may come to dominate the measured capacitance C_m. Hebard *et al.* have shown [225] that, in Al-Al_2O_3-Al trilayer structures, this happens when the oxide thickness falls below 50 Å. We, therefore, expect the bulk capacitance due to C_{60} to dominate the capacitive part of the impedance in the Al-C_{60}-Al trilayer structures with $d_{C_{60}} \sim 1000$ Å that were used in this study (see Sec. 4.6 and Fig. 4-13).

Linearity and time invariance

In addition to the interfacial effects, one needs to keep in mind that, in order to be able to reliably interpret a dielectric measurement, it needs to be performed in the *linear regime*. Whether or not a given sample is linear depends on the applied voltage. Most dielectrics become nonlinear at electric fields on the order of 10^5 V/cm, and experience catastrophic breakdown at electric fields on the order of 10^6 V/cm. Therefore, when dealing with films of thicknesses on the order of 1000 Å (a typical film thickness in our studies), the applied voltage must be kept at ~0.1 V or lower to keep a safe distance of two orders of magnitude or more away from the typical breakdown voltage.

The other important characteristic of a measured dielectric system is its *time invariance*. While usually not a problem at frequencies of 1 Hz and higher, this condition is very difficult to fulfill in very low frequency (VLF) measurements, when a single frequency scan may take hours, or even days. Temperature fluctuation, humidity, diffusion of ambient gases, and sample changes caused by other factors may complicate the interpretation of the results. Therefore, care should be taken to ensure that the sample changes only insignificantly during the interval required to make a single sample measurement.

Cable capacitance

Additional problems are introduced by cabling and shielding issues. In Fig. 3-4, the

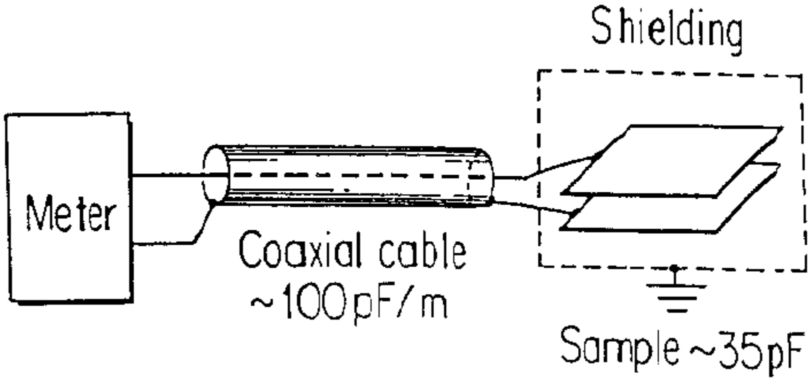

Figure 3-4: Schematic diagram of a measurement system illustrating the effect of cable capacitance and shielding.

parallel-plate sample is connected to a meter by a coaxial cable (~100 pF/m). A 2-meter cable introduces a capacitance of 200 pF in parallel with the sample capacitance, which must be subtracted from the measured capacitance C_m to determine the sample capacitance. Clearly, when the cable capacitance is comparable to the sample capacitance, the sensitivity and accuracy are reduced. It is, therefore, advisable to use the twisted-pair cables whenever possible, as they usually possess smaller capacitance per unit length than the coaxial cables.

Additionally, the cable and electrodes must be shielded, to prevent the pickup at 60 Hz and its harmonics which degrade measurements at or near those frequencies.

3.2.3 Measurement equipment

Whether using parallel plate or other types of electrodes, an AC measurement involves determining the admittance between the electrodes under sinusoidal steady-state conduction. Any AC measurement system thus includes a generator to produce the sinusoidal excitation fed to the sample, and an analyzer to compare the magnitude and phase of the output with the excitation input. The instruments and configurations used in this study are described below.

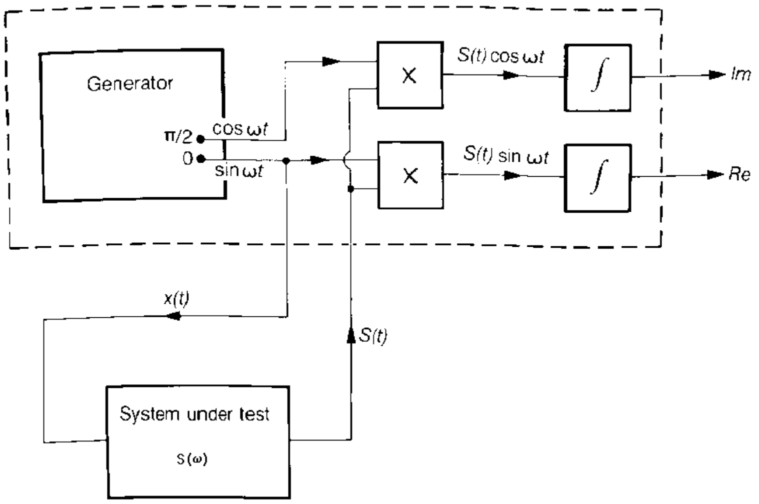

Figure 3-5: A schematic of the working principle of the SI 1254 Frequency Response Analyzer.

HP 4274A LCZ meter

Hewlett Packard's HP 4274A LCZ Meter is a general-purpose impedance-measuring instrument designed to measure circuit components such as capacitors and inductors in the frequency range from 100 Hz to 100 kHz. The magnitude of the sinusoidal input excitation can be varied from 0.01 V to 10 V, and was usually fixed at 0.1 V to ensure that the measurement stays in the linear regime, as discussed above. The instrument is equipped with the standard IEEE 488 computer bus, which facilitates interfacing and control from a lab computer. Appendix A.1 describes the LabView software interfacing the instrument with an IBM-compatible PC.

SI 1254 Frequency Response Analyzer

The Digital Frequency Response Analyzer (FRA) SI 1254 by Solartron Instruments (a division of Schlumberger Ltd.) is an example of the digital correlator system. The principle of transfer function measurement is shown schematically in Fig. 3-5. The sample response $S(t)$ to the perturbing signal $x(t) = X_0 \sin \omega t$ is correlated with two synchronous reference signals, one in phase with $x(t)$ and the other 90^o out of phase, in order to calculate the real and imaginary parts of the sample's transfer function $\mathbf{S}(\omega)$:

$$Re\{\mathbf{S}(\omega)\} \sim \frac{1}{T}\int_0^T S(t)\sin\omega t\, dt \tag{3.5}$$

$$Im\{\mathbf{S}(\omega)\} \sim \frac{1}{T}\int_0^T S(t)\cos\omega t\, dt \tag{3.6}$$

where T, the integration time, is an integer number of periods of the perturbing signal. The FRA thus yields directly the real and imaginary parts of the transfer function of the sample, which, in SI 1254, can alternatively be displayed in the phase–magnitude notation.

Since the input impedance of the SI 1254 FRA is relatively low (100 MΩ), the output signal $S(t)$ needs to be channeled through a high-bandwidth amplifier, such as the SR 570 current amplifier described in Sec. 3.4.[1] Because the FRA is a *digital* instrument, it can be used to perform measurements at arbitrarily low frequencies. In this study, we have measured the dielectric properties of C_{60} films at frequencies as low as 1 mHz. Appendix A.2 presents the LabView software interfacing the SI 1254 FRA with a personal computer.

Other equipment

All of the functions of the FRA can alternatively be implemented directly in a modern personal computer equipped with appropriate Input/Output hardware using digital signal processing techniques. Work has been started on a digital computer-based data acquisition system (DAQ) based on the National Instruments' AT-MIO-16E-3 multifunction I/O board. The board features two analog output channels for generation of the excitation signal, and 16 analog input channels for output detection. The 500 kSamples/s, 12-bit (1 in 4,096) resolution, and 100 GΩ input impedance pro-

[1]The SI 1286 Electrochemical Interface by Solartron Instruments, with input impedance exceeding 10 GΩ, can also be used for signal conditioning.

vide the operational parameters better than those of the SI 1254 FRA. A LabView implementation of the frequency analysis system is currently in progress.

3.3 Microdielectrometry

Clearly, the calibration of the parallel-plate measurements described in Sec. 3.2 will be affected if the plate spacing d changes in the course of the measurements, as it will, for instance, at the C_{60} phase transition point $T_{01} \approx 260$ K (Sec. 1.3.2 and Fig. 1-11), or during intercalation of oxygen and other species into the interstitial spaces of C_{60} solid (Sec. 4.7), or during photopolymerization of a C_{60} film (Sec. 1.3.2).

To avoid this problem, we have used the microdielectrometry technique [226–228] to measure dielectric properties of C_{60} at low frequencies. Instead of using a parallel plate geometry, both electrodes used in the microdielectric measurement are placed on the same surface of an integrated circuit (see Fig. 3-6), and the medium to be studied (C_{60} film) is placed over the electrodes by thermal sublimation in vacuum (Sec. 4.5). The comb electrodes in Fig. 3-6, in contrast to parallel plates, provide a fixed calibration for both ε' and ε'', because electrode size and spacing remain constant even when the sample itself is changing. However, the interdigitated electrode geometry is less efficient than parallel plates in terms of coupling the electric field through the sample medium. To increase the signal to an easily measurable level, some microdielectrometer sensors provide amplification in the form of an integrated field-effect transistor, whose gate electrode is one of the two interdigitated electrodes (called the floating gate; see Fig. 3-6). To compensate for the transistor amplification factor, which would require a complex calibration procedure at each operating temperature, a second identical field-effect transistor is simultaneously fabricated on the same integrated circuit. The second field-effect transistor serves as a reference in a differential feedback circuit, the details of which have been published elsewhere [229]. The net effect of the two-transistor plus feedback circuit combination is that when

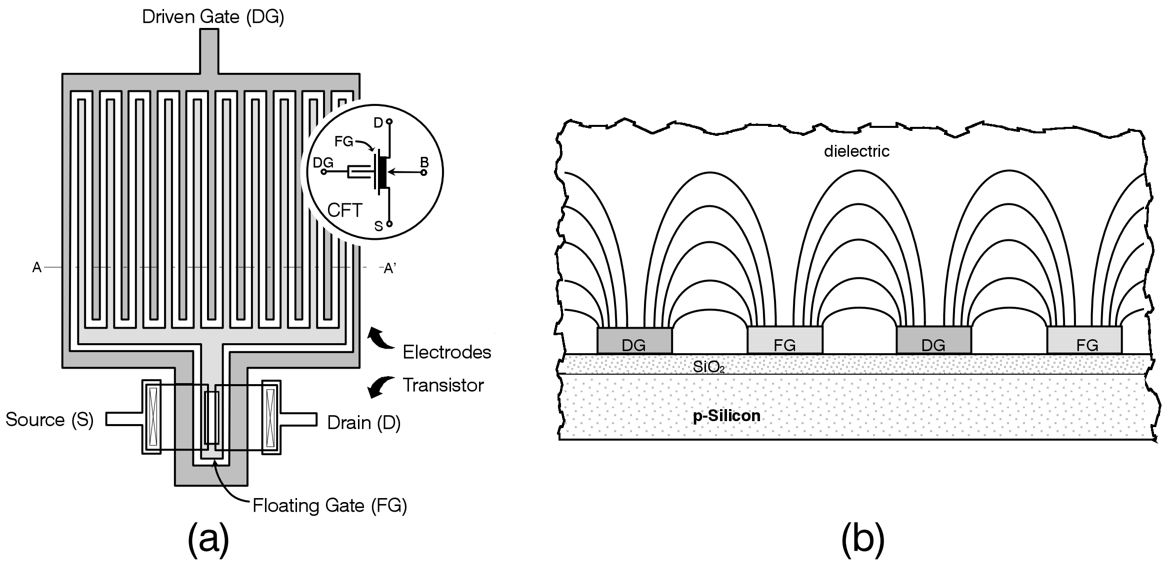

Figure 3-6: (a) Schematic view of active portion of microdielectrometer sensor chip. CFT refers to "floating-gate charge-flow transistor," of which the microdielectrometer is an example. (b) Schematic cross-section through the electrode region (AA′) showing interdigitated driven gate (DG) and floating gate (FG) electrodes, and the electric field coupling them through the dielectric (C_{60}) sample.

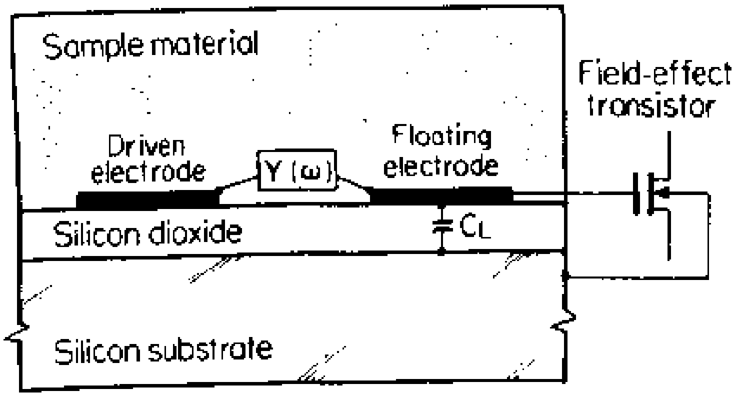

Figure 3-7: Cross section of microdielectrometer sensor. The silicon dioxide insulator is much thinner than the electrode spacing. $\mathbf{Y}(\omega)$ is the comb electrode admittance; C_L is the capacitance between the floating electrode and the substrate [3].

a sinusoidal signal is applied to the driven electrode, the corresponding sinusoidally varying voltage that appears on the floating gate can be measured independent of the transistor amplification factor. This floating-gate voltage has an amplitude and phase relative to the drive signal that depends on the geometry of the device and on the dielectric properties of the sample medium. The fact that the sensing electrode is electrically floating, combined with the proximity of the amplifier to that electrode, means that a good signal-to-noise ratio can be achieved at very low frequencies (down to $\sim 10^{-3}$ Hz).

As the device geometry is both stable and reproducible, the task of calibrating the measurement reduces to relating the measured amplitude and phase for a particular device geometry to the specific values of ε' and ε'' for the sample. To derive this relationship, consider a cross section of the microdielectrometer sensor shown in Fig. 3-7. The cross section shows the electrodes separated from a conducting ground plane (the silicon substrate) by a silicon dioxide insulating layer whole thickness is much less than the electrode spacing. One of the electrodes is driven with a signal, while the other is connected to the input gate of one of the field-effect transistors,

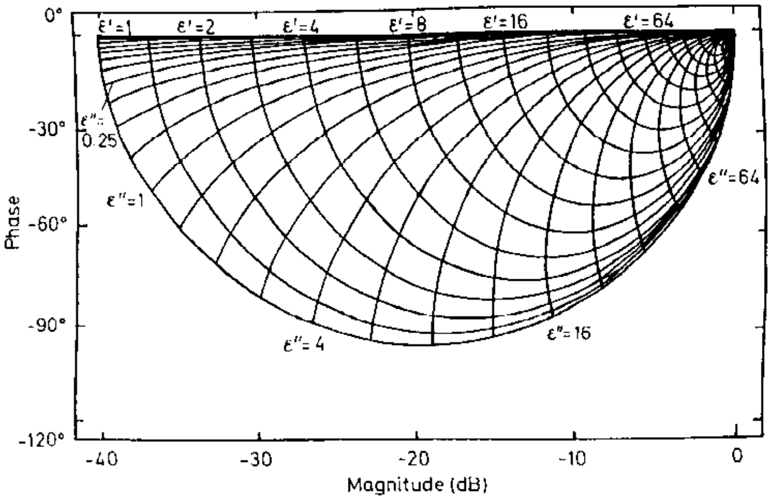

Figure 3-8: Calibration of the microdielectric sensor, showing contours of constant permittivity and loss factor as a function of the measured magnitude and phase [230, 231].

as described above. Except for a capacitance C_L between it and the ground plane, this latter electrode is electrically floating. The capacitance C_L integrates the current reaching the floating electrode through the comb electrode admittance $\mathbf{Y}(\omega)$, and develops a voltage which depends on the charge rather than the current [3]. Therefore, instead of providing a direct measurement of $\mathbf{Y}(\omega)$, the microdielectrometer measures this voltage, or, equivalently, the complex transfer function defined as follows:

$$\mathbf{H}(\omega) = \frac{\mathbf{Y}(\omega)}{1 + j\omega C_L \mathbf{Y}(\omega)}. \tag{3.7}$$

Like the admittance $\mathbf{Y}(\omega)$, the transfer function $\mathbf{H}(\omega)$ has a magnitude and phase which can be interpreted in terms of an assumed homogeneous dielectric medium with permittivity ε' and loss factor ε'', in accordance with a particular model for admittance $\mathbf{Y}(\omega)$ appropriate for the material under study. Figure 3-8 illustrates such a calibration as a contour plot, for the case of $\mathbf{Y}(\omega)$ corresponding to the simple model of Fig. 3-2.

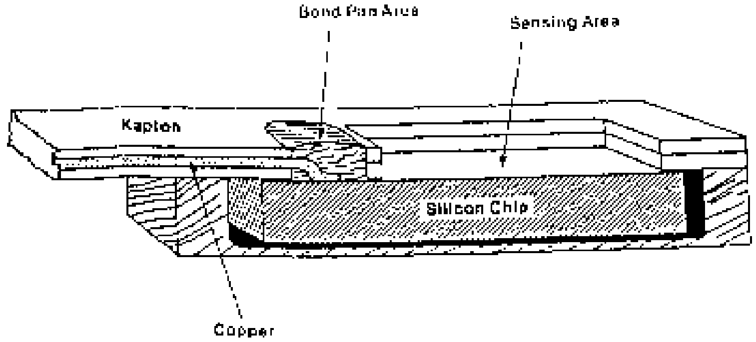

Figure 3-9: Schematic of "ribbon cable" packaging of the Micromet Instruments' integrated sensor (such as the one shown in Fig. 3-6.) The bonds from the package to the chip are completely passivated, and thus are not exposed either to the material under test or to the ambient environment.

Two types of sensors have been used in this study, both supplied by Micromet Instruments Inc. (Newton, MA). The first, used for characterization of the dielectric properties of C_{60} films as function of oxygen diffusion (see Sec 4.4.2), was an integrated sensor shown in Fig. 3-6, having an electrode spacing of 12.5 μm, and oxide (SiO_2) thickness of approximately 1.5 μm, and approximately 7.5 cm of total electrode meander (see Table 3.1). The sensors of this type are preassembled in a "ribbon cable" package, as shown in Fig. 3-9.

The other type of sensor, the so-called "Micron Sensor" that was introduced by Micromet Instruments in 1995, was used for transport and photoconductivity studies of the C_{60} films. It is comprised of two chromium interdigitated electrodes deposited on a quartz substrate (Fig. 3-10). Unlike the sensor in Fig. 3-6, the new Micron Sensor does not have the integrated on-chip electronics, but compensates for the loss of amplification with a more closely packed geometry, featuring 1 μm inter-electrode spacing and a 1 m meander length (see Table 3.1). It is configured so that a variety of material deposition techniques, including spin-coating, spraying, printing, and thermal sublimation, may be used to apply films to the surface of the sensor.

A measurement system that determines the real and imaginary parts of the di-

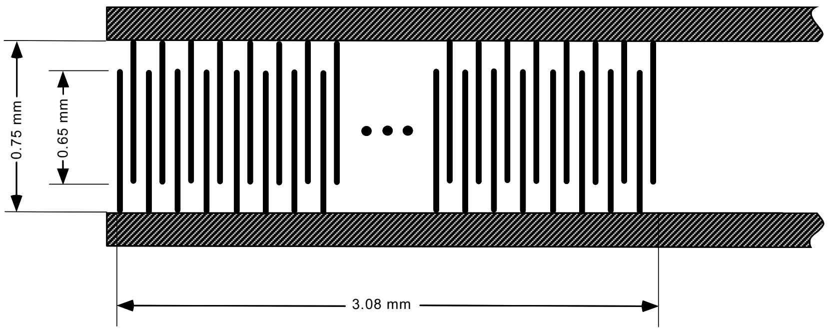

Figure 3-10: The Micron Sensor geometry. Chromium electrodes (1500 Å) are deposited on quartz substrate. [Courtesy of Huan Lee (Micromet Instruments, Newton, MA) and David Day (Auburn International, Denvers, MA).]

Specification	Integrated sensor	Micron sensor
Sensor Dimensions	$14'' \times 0.375'' \times 0.02''$	$1 \times 1 \times 0.04$ cm
Active Face Dimensions	$0.2'' \times 0.1''$	3.08×0.75 mm
Electrode Spacing D_μ	12.5 μm	1 μm
Meander Length L_μ	~7.5 cm	1 m
Electrode Thickness H_μ	N/A	1500 Å (chromium)
Permittivity Range	1 to 40	1 to 20
Log Loss Factor Range	–2 to 3	–2 to 2
Log Conductivity Range (S/cm)	–16 to –5	–13 to –5.5
A/D Ratio	N/A	35
Temperature Range	–100 to 250°C	–150 to 200°C

Table 3.1: Microdielectric sensor specifications. (Source: Micromet Instruments, Inc.)

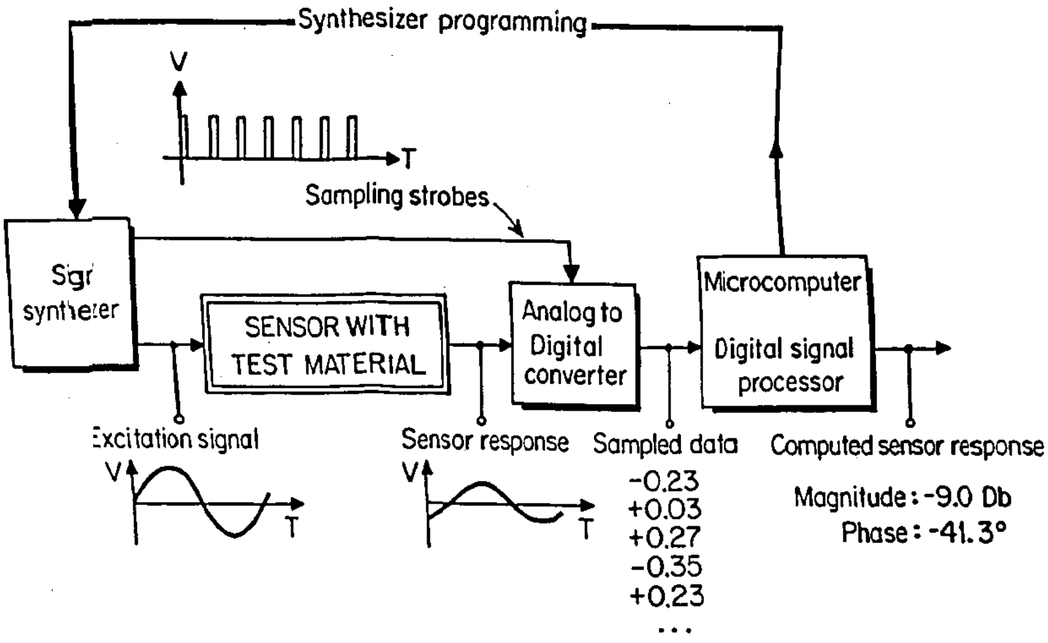

Figure 3-11: Functional block diagram of sampled data system used in microdielectrometry measurements [231].

electric constant of the material coating the sensor consists of a frequency response analyzer (similar to the one described in Sec. 3.2.3) and a device (that can be implemented either in hardware on in software) for converting the measured gain and phase into the real and imaginary parts of the dielectric constant. A calibration table (different for each type of sensor), such as the one shown in Fig. 3-8, is used for the conversion.

For most of our sensor-based dielectric measurements, we used the commercially available *Eumetric® System II Microdielectrometer* by Micromet Instruments, Inc. (Newton, MA) that combines both the FRA and the lookup functions in a single apparatus. It contains a digital correlator [232] that supplies the sinusoidal drive signal to the driven gate electrode and determines the relative amplitude and phase of the comparator output signal. A functional block diagram of the digital correlator is shown in Fig. 3-11. A master clock synchronizes the digitally synthesized drive waveform and the sampling of the comparator output. A discrete Fourier transform (implemented in software) is used to determine the amplitude and phase of the sampled waveform. Based on the accuracy of the amplitude and phase measurement electronics, the ε'' sensitivity of the microdielectrometer is about 0.01 [232], which for a medium having a dielectric permittivity of 4 corresponds to the loss tangent D sensitivity of less than 0.003. At a frequency of 0.01 Hz, an ε'' sensitivity of 0.01 corresponds to a conductivity sensitivity of about 10^{-16} S/cm.

The microdielectrometer was interfaced with an IBM-compatible computer via RS-232 serial port using a versatile LabView software presented in Appendix A.3.

Both the integrated sensor and the Micron Sensor include an on-chip temperature indicator. Since all dielectric and transport properties are temperature dependent, the ability to make a temperature measurement at the same point as the dielectric measurement is a useful feature of the microdielectrometry technique. Together with other unique characteristics of this technique described above (*e.g.*, open-faced electrodes, fixed calibration, good sensitivity), microdielectrometry is particularly appropriate for performing in-situ measurements, investigating the dynamics of diffusion and adsorption, and monitoring the phase transition and cure processes. The results obtained by using this technique for the dielectric and transport studies of C_{60} films are presented in Sections 4.7 and 4.4.2, respectively.

3.4 Transport Measurements

As detailed in Sec. 2.3.4, an independent measurement of the DC conductivity σ_0 is necessary in order to recover the dielectric function $\varepsilon(\omega)$ from the effective dielectric function $\varepsilon_{\text{eff}}(\omega)$ obtained from an AC dielectric measurement. In addition, there are a number of situations where a transport measurement itself provides valuable information about the structure of the sample. For instance, since the resistivity of fullerites has been shown to be extremely sensitive to the presence of oxygen in the interstitials of their fcc lattice (see Sec. 4.4.2), transport measurements can be an effective tool for ascertaining the oxygen content of C_{60} films.

We have seen in Chapter 1 that, in their pristine state, fullerene solids are insulating. The resistivity of pure crystalline C_{60} is $\sim 10^7$ $\Omega\cdot$cm (see Table 1.2), and it can rise by as much as three orders of magnitude as a result of oxygen adsorption. It can easily be shown using Table 3.1 and Fig. 3-10 that, if a Micron sensor is used to measure the resistivity of such an oxygenated C_{60} film, the DC resistance being measured will exceed 1 GΩ. Measuring resistances of this magnitude reliably requires special techniques, which are considered below.

As always in high-resistance measurements, a known voltage should be applied to the sample, and the resulting current should be measured. This approach is commonly referred to as SVMC (Source Voltage Measure Current).[2]

The naïve way of measuring an unknown large resistance R_s is to terminate the circuit with a well-calibrated resistor R_0 of known value, and to amplify the resulting voltage with a voltage preamplifier, as shown in Fig. 3-12(a). In this configuration, R_0 serves both as a reference resistor whose value is known precisely, and as a current-limiting component of the circuit ensuring that, regardless of the value of the test resistor R_s (which may change by many orders of magnitude, as a result of, *e.g.*, oxygen diffusion and temperature changes) the current in the circuit is limited to V_s/R_0. Using a simple voltage divider formula and solving for R_s, we derive the formula for calculating the unknown resistance R_s from the circuit parameters of Fig. 3-12(a):

$$R_s = R_0 \left(G\frac{V_s}{V_m} - 1 \right), \tag{3.8}$$

where G is the differential amplifier gain, and V_m is the measured voltage. While, under certain conditions, this method may yield satisfactory results, it has a number of drawbacks. Most importantly, to get a large voltage from the current I_s, a large

[2]Note that, when dealing with low-resistance (high-conductivity) samples, the Source Current Measure Voltage (SCMV) approach should instead be used.

resistor R_0 is necessary,[3] which, in combination with cable capacitance and other stray capacitance (see below), can lead to unacceptable penalties in frequency response and phase accuracy.

A much better amplitude and phase accuracy in the presence of stray capacitance can be achieved by using a current amplifier, as shown in Fig. 3-12(b). Assuming an ideal (infinite input impedance) linear OpAmp, the unknown resistance R_s is simply

$$R_s = -R_f \frac{V_s}{V_m}, \tag{3.9}$$

where R_f is the feedback resistor. For our measurements, we used the SR570 Low Noise Current Amplifier from Stanford Research (Sunnyvale, CA). A block diagram of the SR570 amplifier is reproduced in Fig. 3-13.

A few special consideration for high-resistance measurements [233] are outlined below:

Settling time. The settling time of the circuit is particularly important when making high-resistance measurements. To illustrate, suppose that a 10 GΩ resistive sample is connected to the measuring instrument with a coaxial cable. Considering that a typical coaxial cable has capacitance of ~100 pF/m, the circuit's settling time will be 10 GΩ $\times$ 100 pF/m = 1 s.

Instrument Loading. Whenever an ohmmeter is used for high resistance measurements, its input impedance must be considered. If an ohmmeter with input resistance R_I is connected to the resistance under test R_s, then the indicated (measured) resistance R_m is

$$R_m = R_s \left(\frac{R_I}{R_s + R_I} \right).$$

[3] In the instances when the configuration depicted in Fig. 3-12(a) was used (in particular, in all transport experiments conducted at MIT), the high precision film resistors from Caddock Electronics, Inc. (Roseburg, Oregon) were utilized. Available in denominations as high as 100 MΩ, these resistors are remarkably robust both with respect to temperature fluctuations and in their frequency response.

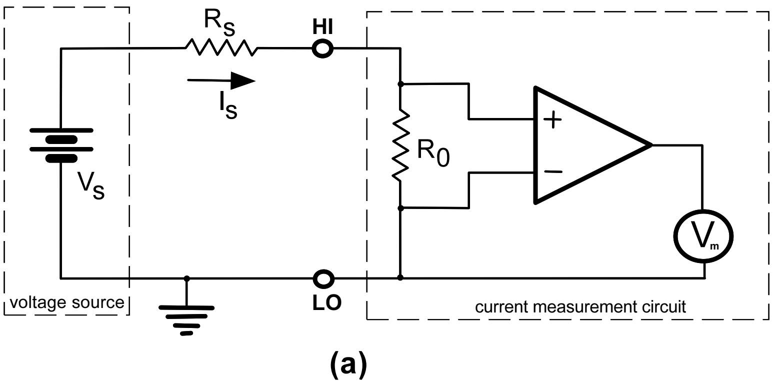

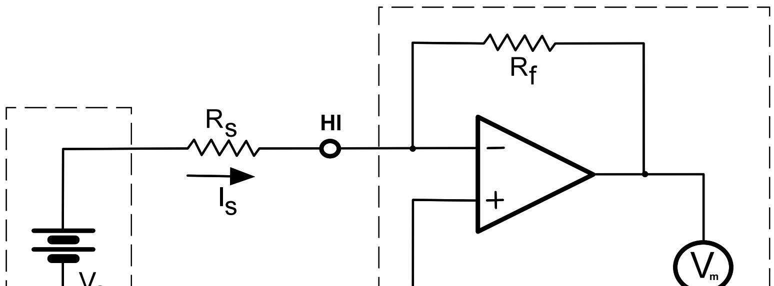

Figure 3-12: (a) A schematic of the current measurement circuit using a large terminating resistor R_0. The voltage drop over R_0 is amplified by a differential OpAmp of gain G, and measured using a voltmeter V_m. (b) A schematic of the current measurement circuit using a current amplifier. The current to voltage conversion gain is controlled by the feedback resistor R_f.

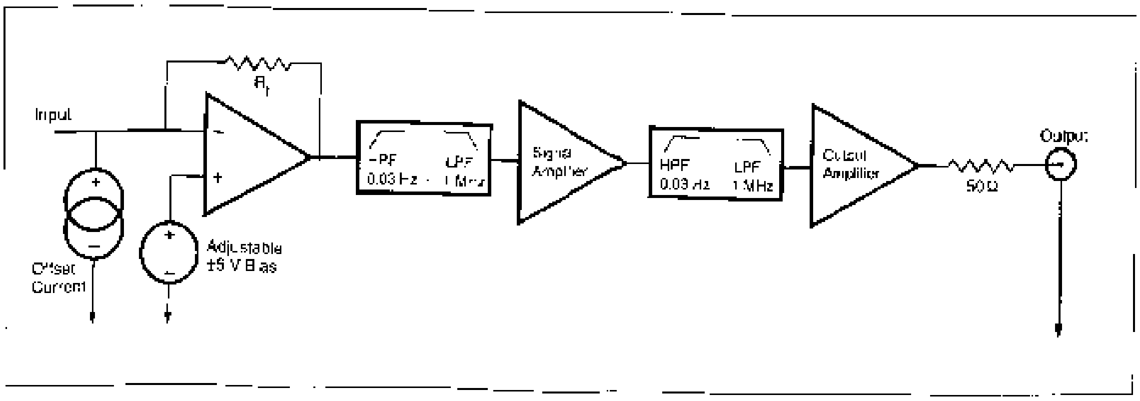

Figure 3-13: A block diagram of the SR570 Low Noise Current Amplifier. The input current can be offset to suppress any undesired background currents. The voltage at the "+" terminal of the amplifier is controlled by an adjustable ± 5 V bias source (0 V at the "+" terminal makes the SR570's input a virtual null). The current to voltage conversion gain is controlled by the feedback resistor R_f. Sensitivities from 1 pA/V to 1 mA/V can be selected in a 1-2-5 sequence. As the sensitivity increases and R_f gets larger, any capacitance present will cause the bandwidth of the instrument to suffer. The SR570 provides a choice between a "high bandwidth" mode, where R_f is chosen as small as possible and the gain is made up later in the amplifier chain, and a "low noise" mode, where R_f is chosen as large as possible to optimize noise performance. The noise performance and frequency response of the instrument can be further adjusted using two identical first order RC filters that can be configured as lowpass, highpass, or bandpass, with the cutoff frequencies controlled from the front panel of the instrument.

Thus, if an ohmmeter with input resistance of 1 GΩ is used to measure a 100 MΩ sample, the resulting measurement will be off by 9%.

Guarding. Guarding high-resistance test connections can significantly reduce the effects of leakage resistance, increase measurement accuracy, and improve time response (bandwidth) of the instrument. Under this technique, the measurement cable shield is driven with a unity gain amplifier to maintain the same potential as the wire inside the shield. Since both the shield and the wire are then at the same potential, the leakage current is eliminated. Most modern instruments provide a guard terminal facilitating this technique.

Leakage Currents. In the SVMC configurations, such as the one pictured in Fig. 3-12(b), care should be taken to suppress any leakage currents present in the system. The *baseline suppression* feature of the SR570 amplifier (see Fig. 3-13) is available to offset the input current so as to suppress any undesired background currents.

Provided that the difficulties outlined above are addressed and a successful measurement has been performed, the output of the current amplifier (ranging from -5 V to +5 V for SR570) needs to be converted to the resistivity of the sample being measured. For samples in the parallel-plate configuration (Fig. 3-1), this is merely a matter of plugging in the electrode area A and separation distance d into the formula

$$\rho = R_s \frac{A}{d}, \tag{3.10}$$

where R_s is the sample resistance calculated using Eqn. (3.9). In practice, instead of the Eqn. (3.9), amplifier gain G_{amp} and output voltage V_{amp} are used to calculate R_s:

$$R_s = \frac{V_s}{G_{\mathrm{amp}} V_{\mathrm{amp}}}. \tag{3.11}$$

Note that the amplifier gain G_{amp} is expressed in *amperes per volt* (A/V).

The situation gets somewhat more complex when the Micron sensor (see Sec. 3.3) is utilized to measure the resistivity. The sensor's geometrical parameters listed in Table 3.1 should then be used to calculate the geometrical factor A/d of Eqn. (3.10). For films thicker than the sensor electrode thickness H_μ,

$$\frac{A}{d} = \frac{L_\mu H_\mu}{D_\mu}, \tag{3.12}$$

where L_μ and H_μ are, respectively, the meander length and the electrode spacing of the sensor. Given the parameters in Table 3.1, we calculate

$$\frac{A}{d} = 15\text{cm}.$$

Clearly for films thinner than H_μ, the film thickness d_{film} should be used in place of H_μ in Eqn. (3.12).

Note that, when the Micron sensor is used to measure the dielectric properties of materials, the geometrical parameter A/d can be used to calculate the dielectric constant ε' from the measured capacitance C_m:

$$\varepsilon' = \frac{C_m}{A/d}. \tag{3.13}$$

However, the simple-minded way of calculating A/d utilized in Eqn. (3.12) is no longer adequate, since it does not take into account the fringing fields imposed by the geometry of the sensor (see Figs. 3-6 and 3-10), which cannot be neglected in AC measurements. Micromet Instruments recommends using A/d = 35 cm, a value determined from experimental calibrations. In assessing the merits of this value relative to the approximation of Eqn (3.12), it is important to keep in mind that, in dielectric measurements, the fringe fields extend not only above the surface of the sensor into the bulk of the measured material, but also into the quartz substrate, whose dielectric constant $\varepsilon'_{\text{quartz}} = 3.75$ contributes additional polarization (which we consider to be frequency-independent) that gets internalized in the A/d geometrical parameter.